JOURNAL OF PROPULSION AND POWER
Vol. 27, No. 3, May–June 2011

Poisson Ratio Effect on Stress Behavior of Propellant Grains Under Ignition Loading

Hung-Ta Chu* and Jung-Hua Chou†
National Cheng–Kung University, Tainan City 70701, Taiwan, Republic of China

DOI: 10.2514/1.50249

In this study, a transient finite element model, accompanied by the time-temperature shift principle, is used to simulate the transient response of a solid rocket motor so that the response of the propellant grains under real ignition pressurization loading conditions is investigated. The results show that the transient effect is important for structural completeness of the solid propellant grains under the ignition loading conditions. There is an apparent difference among the stresses of different Poisson's ratios. When changing the property of propellant grains from compressible into incompressible, the stress and strain of propellant grains under ignition pressurization loading decreased significantly. The stress variation versus Poisson's ratio is nonlinear and cannot be neglected.

I. Introduction

IN THE last three decades, more and more attention has been paid to the design, manufacturing, and evaluation of solid propellant grains in order to meet service life and performance requirements. As a result, great progress has been made in the design of solid propellants. Currently, the structural design of a solid rocket motor (SRM) is based on the concept of a mechanically weak solid propellant grain cast into a stronger metallic or composite case. The outer case provides the needed resistance for maintenance and operational loads, whereas the inner propellant grain's low strength is used to transmit loads from the grain surface to the outer case.

It is well known that, under loading conditions, cracks can develop in solid propellants due to the excessive loads. In a missile system, the structural configuration of a SRM is one of the most complicated parts. Thus, numerical techniques are usually adopted to simulate its physical behavior and evaluate the structural integrity of different designs so that product development cost and cycles can be reduced. To predict the changes in stress and strain variations with time, transient analysis is essential. The finite element method (FEM) [1] is considered as one of the useful computer-aided engineering design tools among different numerical approaches. In the past, various attempts were made to accurately model the structural properties of propellant grains [2]. A chamber was designed for aluminum droplet combustion [3] so that pressures and temperatures in the motor grain could be obtained.

It was recognized that the pressure under charge burning of a propellant was the key point in propellant failure [4]. In evaluating the time-temperature-dependent behavior of incompressible polymer materials, the time-temperature shift principle, reduced integration, and thermorheologically simple material assumptions were widely adopted in linear transient analysis [5]. The temperature of the insulation layer of the SRM was computed, the data were applied for the finite element analysis [6], and commercial finite element software was used for ignition pressure analysis [7]; furthermore, from experimental observations, both high pressures and temperatures occurred along the solid surface and caused cracks in the propellant grains or in the separation region between the propellant and the inhibitor or the liner [8]. By using the commercial finite element package, the thermal load and internal pressure load are applied to obtain a more accurate time-dependent viscoelastic solution [9]. As far as the solid propellant grain design is concerned, it is difficult and laborious in predicting the physical response during the design phase. Therefore, using computer simulation techniques to analyze the structural behavior of SRM in the preparatory design stage is very necessary.

II. Simulation and Finite Element Modeling

The purpose of transient response analysis is to capture the behavior of a structure subjected to time-varying loads, with all of the forces applied to the structure being known at each time instant. As the structure moves in response to the applied load, forces in the individual components are induced. In this study, the direct transient response analysis is applied to examine the ignition process due to its efficient performance in solving the equations without the need of a small time step.

Modern solid propellant grains contain an elastic binder, which is saturated with a high level of solid particles. Its behaviors under loading are complicated, including interfacial debonding, microvia formation, temperature and pressure dependence, large deformation, stress softening, etc. To simplify the analysis, a proper constitutive model [10,11] of the solid propellant grains for engineering analysis is adopted in this study.

In this study, the behavior of the hydroxyl-terminated polybutadiene binder (HTPB) propellant is examined. Its experimentally deduced master relaxation modulus versus the temperature-reduced time is shown in Fig. 1 [12]. The corresponding time-shift factor is shown in Fig. 2 [12]. The curves in both figures are obtained from the experimental data at different ambient temperatures. Propellant failure properties are used on master curves of the maximum nominal stress $\sigma_{\max}$ and strain at the maximum nominal stress $\varepsilon_{\max}$ versus the temperature-reduced time $\frac{t}{a_T}$. The tests used to generate the master curves are conducted in accordance with the Joint Army–Navy–NASA–Air Force Tentative Standard Uniaxial Test Procedure [13]. The time-temperature shift factor a_T obtained from the relaxation standard for the solid propellant grains depends on its allowable stress and strain. The strength of the HTPB propellant used in this study is obtained from the master allowable stress and strain curves, shown in Figs. 3 and 4 [12].

To predict the stress and strain response in detail for the ignition process, the ANSYS 20-node viscoelastic model with 5040 grid nodes and 4200 8-node elements, as shown in Fig. 5, are built to acquire the stress and strain results. A number of structural analyses based on the number of elements, as indicated in Fig. 6, are conducted to see the corresponding effect of principal stress attained during the analysis. This maximum principal stress attained is then considered as the basis for mesh refinement. As shown in Fig. 6, it is

Received 8 April 2010; revision received 2 August 2010; accepted for publication 5 August 2010.

*Graduate Student, Department of Engineering Science; currently Assistant Researcher, Chung Shan Institute of Science and Technology, P. O. Box 90008-21-4, Manzhou, Pingtung, 94744, Taiwan, Republic of China.

†Professor, Department of Engineering Science.

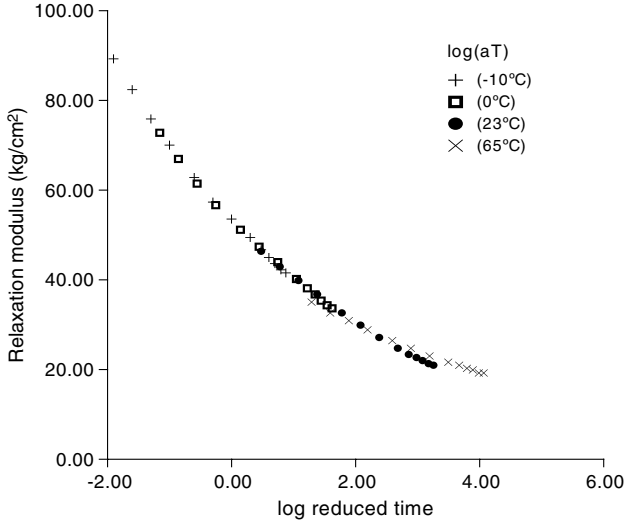

Fig. 1 Master curve of the relaxation modulus for the HTPB propellant.

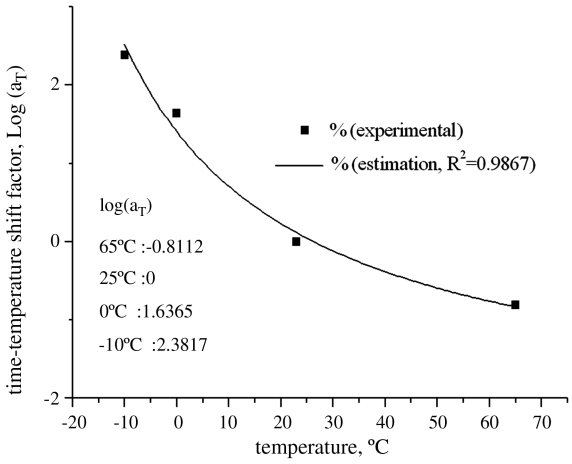

Fig. 2 Time-shift factor for the HTPB propellant.

clear that no further increase in effective stress is achieved if the number of elements is increased beyond 5040. The relative error for the prediction of the strength ratio for the maximum stress criterion between the mesh with 5040 elements and a refined mesh with 6000 elements was less than 1%. The mesh with the number of elements

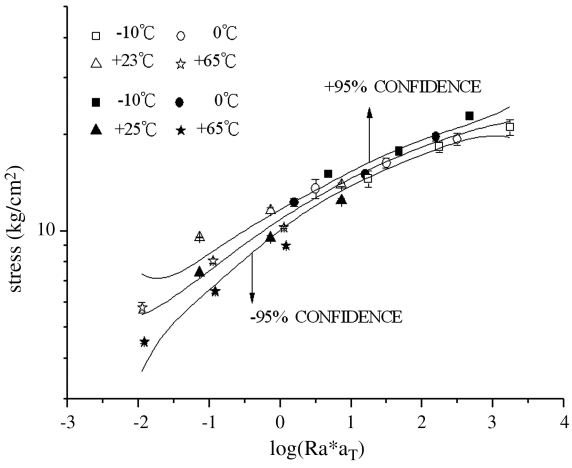

Fig. 3 Master curve of the allowable stress for the HTPB propellant.

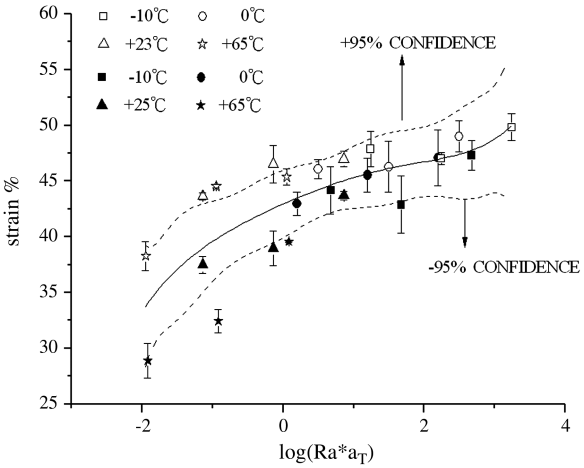

Fig. 4 Master curve of the allowable strain for the HTPB propellant.

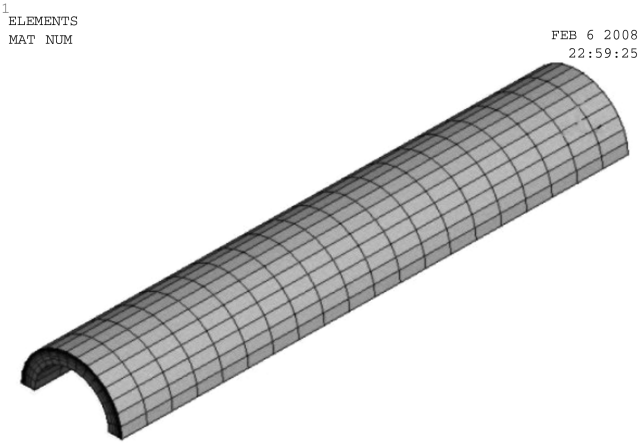

Fig. 5 FEM of the solid propellant grain.

indicated in Fig. 6 is then considered for the analysis in order to get the mesh-independent results [14,15]. Conventionally, the Poisson ratio of $\nu \fallingdotseq 0.5$ is used to approximate the propellant grain incompressibility. However, when ν approaches the value of 0.5, the stresses depends strongly on ν; namely, stresses may double its value

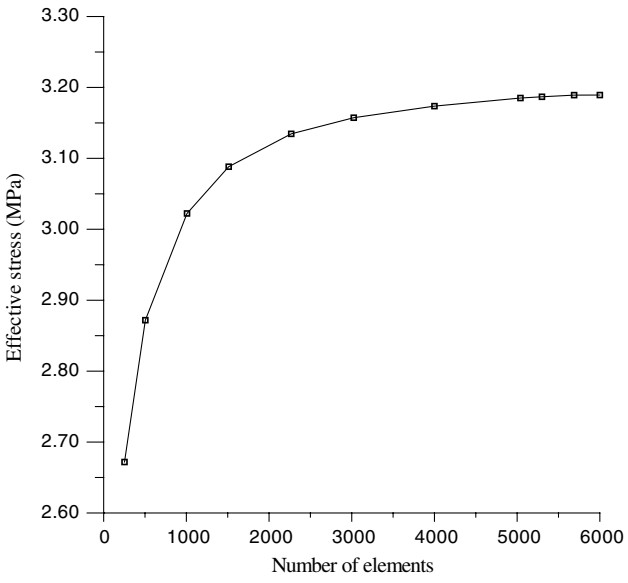

Fig. 6 Mesh sensitivity analysis based on effective stress attained.

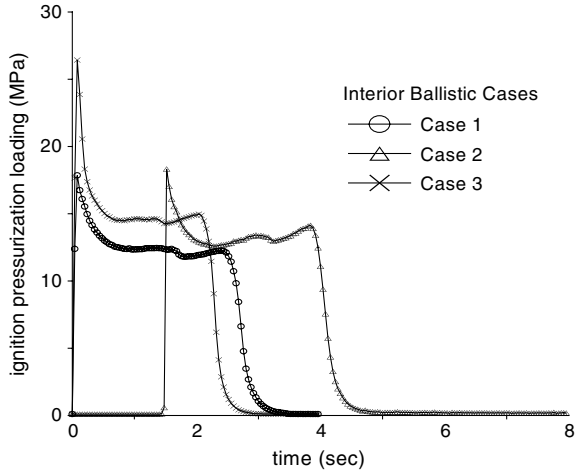

Fig. 7 Ignition pressurized loading (cases 1, 2, and 3).

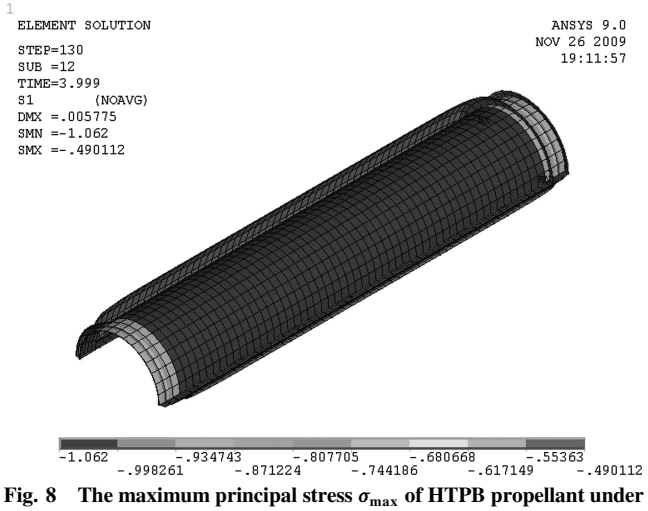

Fig. 8 The maximum principal stress σ_{max} of HTPB propellant under ignition pressurized loading case 1 (DMX denotes maximum deflection, SMN denotes minimum solution value, and SMX denotes maximum solution value).

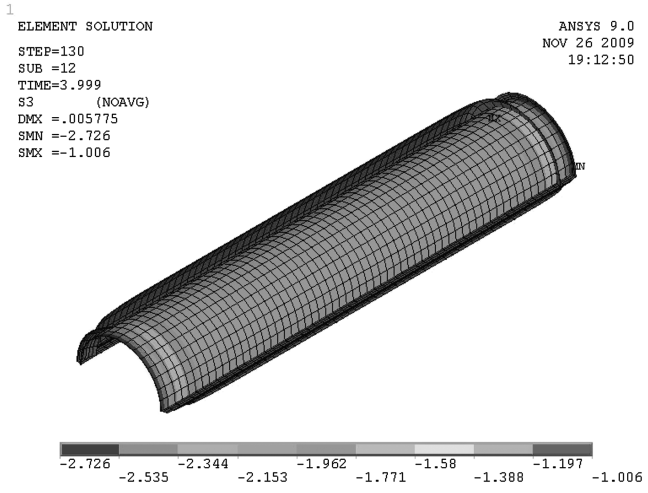

Fig. 9 The minimum principal stress σ_{min} of HTPB propellant under ignition pressurized loading case 1.

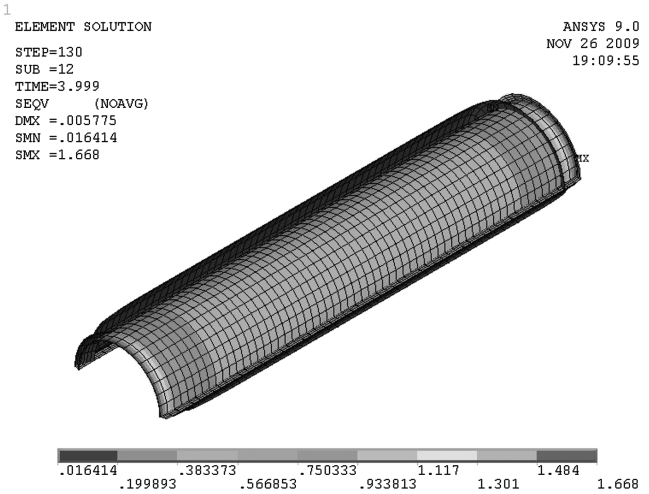

Fig. 10 The effective stress σ_{eff} of HTPB propellant under ignition pressurized loading case 1.

as ν varies from 0.489 to 0.499. Therefore, in this investigation, a FEM [16] of solid propellant grains considering the effect of Poisson's ratio variation was carried out using a FEM analysis, and the formulation is similar to that of Herrmann's [17].

In general, the ignition pressure in a propellant rocket motor always leads to a compressive hydrostatic pressure load throughout the grain. The compressive pressure typically consists of two phases: precipitous rise and conservative decrease. The real pressurization profile depends strongly on the design of the SRM. In the present study, three interior ballistic experimental conditions given in Fig. 7, denoted by cases 1, 2, and 3, respectively, to represent different pressurized processes are used for the transient analysis. Specifically, case 1 represents a smooth ignition condition and case 2 denotes a delayed case because the igniter is not ignited on time, whereas case 3 is a condition with an abrupt increase of the burning interface inside the solid propellant, and it causes the sudden rise of the ignition pressure and the decrease of the reaction time.

III. Simulation Results and Discussion

A. Effect of Incompressible Material on Stress Distribution Under Pressurized Loading

Under the ignition pressurized loading condition of case 1, depicted in Fig. 7, the maximum principal stress σ_{max} of the HTPB propellant, shown in Fig. 8, is -0.490 MPa, whereas the minimum principal stress σ_{min} shown in Fig. 9 is -2.726 MPa and the effective stress σ_{eff} depicted in Fig. 10 is 1.668 Mpa.

For comparison, the simulation results for the three cases shown in Fig. 7 are summarized in Table 1, in which the maximum principal stress, the minimum principal stress, and the effective stress of the HTPB propellant are presented, and the results show two features using loading case 1 as the reference case in Table 1. First, case 2 with delayed ignition causes higher compressive and effective stresses than case 1. Second, there is a 90% difference in the effective stress between cases 1 and 3 due to an abrupt increase of the burning interface inside the solid propellant throughout the reaction process. It should be noted that the critical areas are located at both sides of the solid propellant grain.

Table 1 Stress under different ignition loadings

	σ_{min}, Mpa	σ_{max}, Mpa	σ_{eff}, Mpa
Loading case 1	−0.490	−2.726	1.668
Loading case 2	−0.515	−2.917	1.726
Loading case 3	−0.943	−4.462	3.183

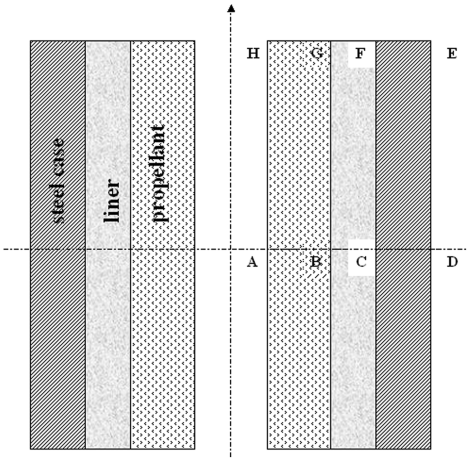

Fig. 11 Cross-sectional diagram of the SRM.

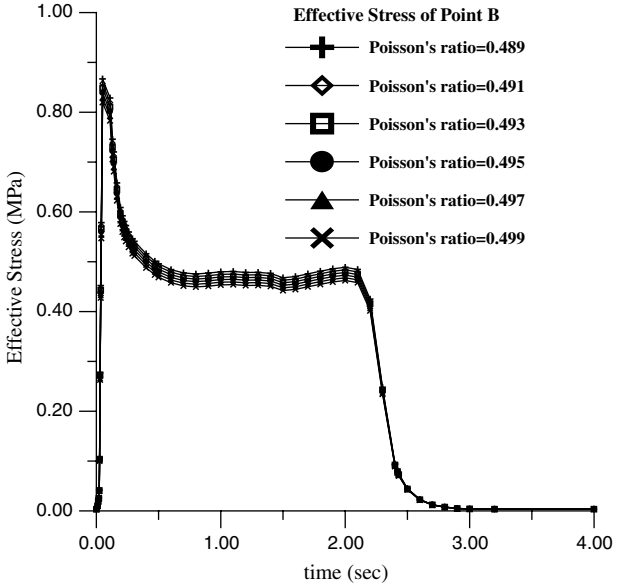

Fig. 12 Maximum effective stress at point B for different Poisson ratios.

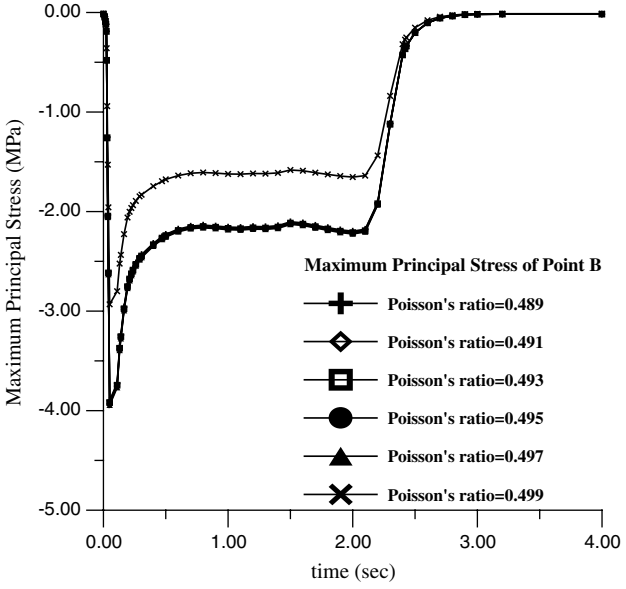

Fig. 13 Maximum principal stress at point B for different Poisson ratios.

B. Effect of Poisson's Ratio on Stress Distribution Under Pressurized Loading

As the ignition pressurized loading condition of case 3 causes the greatest stresses, it is chosen to further investigate the effect of Poisson's ratio on stress variations. Two reference locations are examined. One is along the motor transect of the propellant grain, denoted by CF, and the other is along the radial direction from the propellant grain to the steel case, denoted by AD in Fig. 11. Figure 12 illustrates the maximum effective stress of point B versus time. Please note that point B is at the interface of the liner and the propellant along AD. The maximum effective stress increases rapidly to reach a peak in a relatively short time and then also decreases rapidly to a level value, which holds for a relatively longer time period, and then finally relaxes to zero. As ν increases, the maximum effective stress decreases but is not significantly different.

On the other hand, the trend of the maximum principal stress of point B shows a different behavior, as shown in Fig. 13. Its values coincide together as ν increases from 0.489 to 0.497; namely, ν has an insignificant influence. However, as ν increases from 0.497 to 0.499, it shows an abrupt change; that is, the value of the compressive stress reduces with a further increase in ν.

By contrast, the corresponding stress behaviors for point C, also along AD, are shown in Figs. 14 and 15 for the effective and principal stresses, respectively. In this case, point C is at the interface of the liner and the steel case. By comparing the results shown in Fig. 11, the general trend is the same for these two locations. On the other hand, there are two distinct features for those shown in Fig. 14. First, the stress levels are considerably higher for point C, showing the material effect. Second, the decrease in the stress level with increasing ν is more obvious for point C than point B. By comparing the results shown in Figs. 13 and 15, it can also be observed that the overall trend is the same for points B and C. However, the principal stress at point C is higher than that at point B, similar to the behavior of effective stress. Furthermore, unlike point B, the influence of ν is gradual and noticeable for ν from 0.489 to 0.497, instead of insignificance as at point B. Then there is a large jump of the effective stress for ν from 0.497 to 0.499, as in the case of point B. In other words, for both points B and C, the maximum principal stress has a larger change during the ignition period when ν varies from 0.497 to 0.499.

For the purpose of further comparison, the effective stress at point F is shown in Fig. 16. Location F is at the interface of the liner and the steel case along CF. By comparing these results to those of point C, it is clear that the trend is the same as that at the same material interface. However, the effective stress of F is about twice as big as that at point C, indicating the edge-constrained effect.

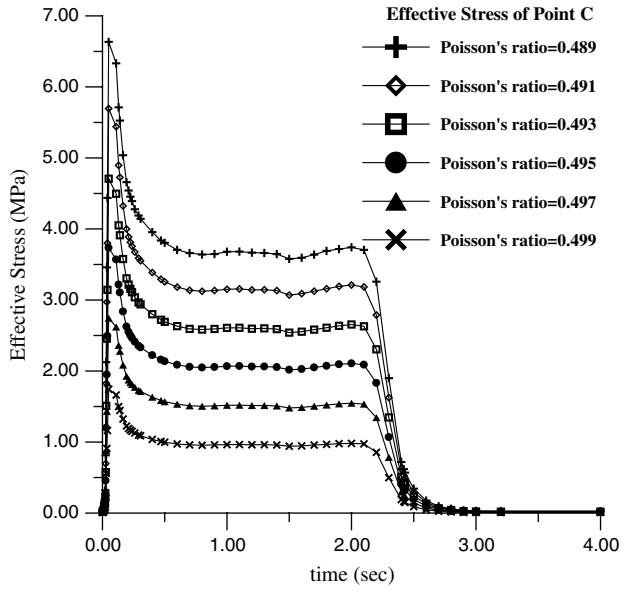

Fig. 14 Maximum effective stress of point C in different Poisson's ratio.

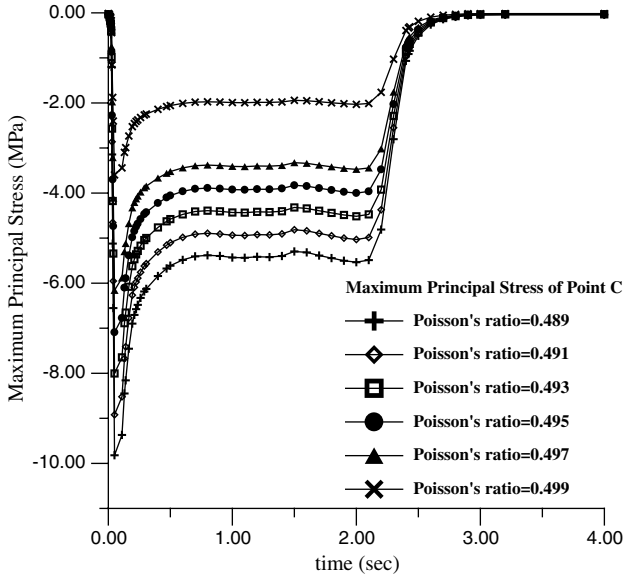

Fig. 15 Maximum principal stress of point C in different Poisson's ratio.

From the previous observations, it is clear that the stress distributions along the SRM along both axial and radial directions are not uniform, due either to edge constraints or material difference. In addition, the usual assumption of the Poisson ratio $\nu \fallingdotseq 0.5$ has to be clarified. Namely, one needs to be cautious about the effect of the Poisson ratio. The present results show that the effect can be either significant or insignificant, depending on the locations and the type of stress examined. However, in most cases, especially the maximum principal stress, a large change in stress level occurs when ν changes from 0.497 to 0.499 and the value of the compressive stress reduces. In other words, the assumption of $\nu \fallingdotseq 0.5$ will underestimate both the maximum effective stress and the maximum principal stress.

Conventionally. the value of solid propellant grains is assumed to be a constant to simplify the experimental task, but the real ν value is from 0.48 to 0.499, depending on the chemical design of the solid propellant grains. In this study, results show that the Poisson ratio variation effect is very important for the structural integrity of solid propellant grains, and the stress and strain responses versus the Poisson ratio variation are nonlinear because the type of polymer material is changed from incompressible to compressible. Therefore,

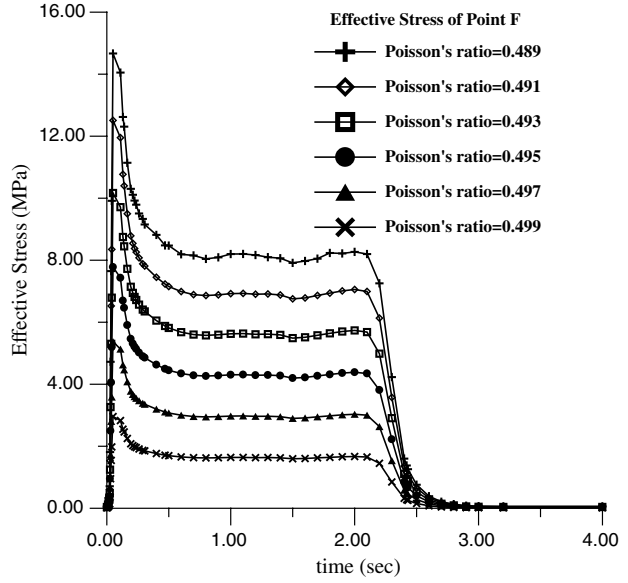

Fig. 16 Maximum effective stress of point F in different Poisson's ratio.

unlike metallic structures, an exact value of the Poisson ratio for polymer materials is very important, and an improper assumption $\nu \fallingdotseq 0.5$ may cause the structural integrity of a missile system subjected to pressure loading to be wrongly evaluated.

IV. Conclusions

To simulate the transient stress behavior of solid propellant grains under ignition pressurization loadings, a three-dimensional FEM accompanied by the time-temperature shift principle was used in this study. Three types of ignition pressurization loading histories were examined to investigate the pressurization loading effect. In addition, six different Poisson's ratio values from 0.489 to 0.499 were studied.

The results show that the effect of the Poisson ratio can be significant. In most cases, both the maximum effective stress and the maximum principal stress exhibit a large change when the value of the Poisson ratio changes from 0.497 to 0.499 with a large reduction in the value of the compressive stress. The conventional approach of assuming the Poisson ratio of $\nu \fallingdotseq 0.5$ (incompressible) for solid propellant grains will underestimate the stress levels of SRMs, as the compressibility has a large effect on the transient stress behavior when $\nu < 0.5$ (compressible).

References

[1] Chen, J. T., and Leu, S. Y., "Finite Element Analysis, Design and Experiment on Solid Propellant Motors with a Stress Reliever," *Finite Elements in Analysis and Design*, Vol. 29, No. 2, 1998, pp. 75–86. doi:10.1016/S0168-874X(98)00015-8

[2] Montesano, J., Kamran, B., Greatrix, D. R., and Zouheir, F., "Internal Chamber Modeling of a Solid Rocket Motor: Effects of Coupled Structural and Acoustic Oscillations on Combustion," *Journal of Sound and Vibration*, Vol. 311, Nos. 1–2, 2008, pp. 20–38. doi:10.1016/j.jsv.2007.08.030

[3] Melcher, J. C., and Rodney, L. B., and Herman, K., "Combustion of Aluminum Particles in Solid-Rocket Motor Flows," *Solid Propellant Chemistry, Combustion, and Motor Interior Ballistics*, Vol. 185, Progress in Aeronautics and Astronautics, AIAA, Reston, VA, 1999, pp. 723–747.

[4] Uluntsev, Y. G., and Merkulov, A. A., "Numerical Calculation of Pressure in a Perforated Well Under a Propellant Charge Burning," *Journal of mining science*, Vol. 43, No. 6, 2007, pp. 592–599. doi:10.1007/s10913-007-0064-9

[5] Solid Propellant Grain Structural Integrity Analysis, NASA SP 8073, 1973.

[6] Zhang, T., and Sun, B., "Numerical Computation of Solid Rocket Motor Insulation Layer Temperature by Finite Element Method," *Journal of Aerospace Power*, Vol. 24, No. 6, 2009, pp. 1407–1412.

[7] Püskülcü, G., and Ulas, A., "3-D Grain Burnback Analysis of Solid Propellant Rocket Motors, Part 1: Ballistic Motor Tests," *Aerospace Science and Technology*, Vol. 12, No. 8, 2008, pp. 579–584. doi:10.1016/j.ast.2008.02.001

[8] Renganathan, K., Nageswara, R. B., and Jana, M. K., "Failure Pressure Estimations on a Solid Propellant Rocket Motor with a Circular Perforated Grain," *International Journal of Pressure Vessels and Piping*, Vol. 76, Nos. 14–15, 1999, pp. 955–963. doi:10.1016/S0308-0161(99)00070-8

[9] Renganathan, K., Nageswara, R. B., and Jana, M. K., "An Efficient Axisymmetric Hybrid-Stress-Displacement Formulation for Compressible/Nearly Incompressible Material," *International Journal of Pressure Vessels and Piping*, Vol. 77, No. 11, 2000, pp. 651–667. doi:10.1016/S0308-0161(00)00042-9

[10] Christensen, R. M., *Theory of Viscoelasticity: An Introduction*, Academic Press, New York, 1982.

[11] Ferry, J. D., *Viscoelastic Properties of Polymers*, 3rd ed., Wiley, New York, 1980.

[12] Solid Propellant Grain Master Relaxation Modulus Analysis, Chung Shan Inst. of Science and Technology, SA 10958-02, Taiwan, ROC, 2001.

[13] "Minimum Standard Structural Analysis Procedures for Solid Rocket Grains Under Thermal and Pressurization Loading," *JANNAF Solid Propellant Structural Integrity Handbook*, Chemical Propulsion Information Agency, Doc. 230, Columbia, MD, 1987.

[14] Krack, M., Secanell, M., and Mertiny, P., "Cost Optimization of Hybrid Composite Flywheel Rotors For Energy Storage," *Structural and Multidisciplinary Optimization*, Vol. 41, No. 5, 2010, pp. 779–795.

doi:10.1007/s00158-009-0469-y
[15] Dar, N. U., Qureshi, E. M., and Hammouda, M. M. I., "Analysis of Weld-Induced Residual Stresses and Distortions in Thin-Walled Cylinders," *Journal of Mechanical Science and Technology*, Vol. 23, No. 4, 2009, pp. 1118–1131.
doi:10.1007/s12206-008-1012-6
[16] Zienkiewicz, O. C., and Morgan, K., *Finite Elements and Approximation*, Wiley, New York, 1983.
[17] Herrmann, L. R., "Elasticity Equations for Incompressible and Nearly Incompressible Materials by a Variational Theorem," *AIAA Journal*, Vol. 3, No. 10, 1965, pp. 1886–1900.
doi:10.2514/3.3277

K. Frendi
Associate Editor